Temperature-Dependent Structure-Property Relationship in $[(4AMTP)PbBr_2]_2PbBr_4$ Single Crystal

A Thesis

submitted to

Indian Institute of Science Education and Research Pune in partial fulfilment of the requirements for the BS-MS Dual Degree Programme

by

Shingote Ajinkya Sundarnath

Indian Institute of Science Education and Research Pune

Dr. Homi Bhabha Road,

Pashan, Pune 411008, INDIA.

April, 2024

Supervisor: Prof. Angshuman Nag

Professor, Department of Chemistry

IISER Pune

Certificate

This is to certify that this dissertation entitled “Temperature-dependent Structure-property Relationship in $[(4AMTP)PbBr_2]_2PbBr_4$ Single Crystal” towards the partial fulfilment of the BS-MS dual degree programme at the Indian Institute of Science Education and Research, Pune represents study carried out by Shingote Ajinkya Sundarnath at Indian Institute of Science Education and Research under the supervision of Prof. Angshuman Nag, Professor, Department of Chemistry, during the academic year 2023-2024.

Angshuman Nag

Prof. Angshuman Nag

Committee:

Prof. Angshuman Nag

Dr. Pramod Pillai

This thesis is dedicated to my grandmother **Sitabai Pachpute**

Declaration

I hereby declare that the matter embodied in the report entitled “Temperature-Dependent Structure-Property Relationship in $[(4AMTP)PbBr_2]_2PbBr_4$ Single Crystal” are the results of the work carried out by me at the Department of Chemistry, Indian Institute of Science Education and Research, Pune, under the supervision of Prof. Angshuman Nag and the same has not been submitted elsewhere for any other degree. Wherever others contribute, every effort is made to indicate this clearly, with due reference to the literature and acknowledgement of collaborative research and discussions.

Shingote Ajinkya Sundarnath

Date: 27/03/2024

Table of Contents

List of Tables

List of Figures

Abstract

Metal halide perovskites are known for their excellent optoelectronic properties. 2D (layered) metal halide perovskite has impressive structural diversity. Due to its structural diversity and facile synthesis, they are considered a good candidate for synthesizing novel 2D halide perovskites with multiple functionalities. Based on the same principle, we have prepared centimetre sized crystals of $[(4AMTP)PbBr_2]_2PbBr_4$ 2D perovskite having hybrid A-site cation using reported antisolvent method. It is expected that the hybrid A-site cation layer, either directly, or indirectly through structural modification, would affect the optoelectronic properties of $[(4AMTP)PbBr_2]_2PbBr_4$. So, the exploration of the temperature-dependent structure-property relationship of this newly discovered 2D perovskites is highly desired.

Since the full chemical space for this structure-type is not yet revealed, the major emphasis of this thesis is devoted to establish structure-property relationship of this newly discovered 2D perovskite. Single crystal x-ray diffraction, variable temperature powder x-ray diffraction, thermogravimetric analysis, and differential scanning calorimetry measurements has been carried out to understand role of hybrid cation in determining temperature dependent structural parameters and phase transition.

Further monoclinic phase of $[(4AMTP)PbBr_2]_2PbBr_4$ 2D perovskite has been studied for their optical properties at cryogenic temperatures to determine possibility of long lived dark excitonic emission that has been generalized for thin films of all monoclinic phase 2D perovskites. The obtained results have been described in terms of three state model established in prior literatures.

Acknowledgments

I want to express my heartfelt thanks to Prof. Angshuman Nag for giving me the opportunity to work on my final year thesis project under his guidance. His critical thinking, collaboration and communication skills really helped me with various scientific challenges encountered during my thesis. His technical proficiency and extensive knowledge of optoelectronics have made me more interested in this research field. His mentorship played a significant role in helping me develop the capabilities needed to thrive in a professional research setting, one that was unfamiliar to me.

Furthermore, I wish to convey my gratitude to my thesis advisory committee member Dr. Pramod Pillai for his invaluable guidance during the mid-year presentation. His support was crucial in helping me understand what was necessary to achieve the desired results in my thesis.

I am especially grateful to Mr. Parikshit Kumar Rajput for solving single crystal data. This is by far most valuable input to my thesis. I also appreciate Mr. Habibul Arfin and Ms. Taniya Dutta for teaching me about solid-state PL measurements during my thesis.

I want to express my heartfelt gratitude to my incredibly supportive lab colleagues: Habibul Arfin, Parikshit, Sajid, Barnali, Srijita, Taniya, Urmila, Animesh, Manmayuri, Vijay, Pavithra and lab post-docs: Parshurama, Yogesh and Ujjal. Working with such wonderful and interactive individuals made every day of my final year thesis a joyful experience. The delightful tea session and group discussion not only added enjoyment to my days but also offered valuable insights that enriched both my personal and professional growth.

I also extend my gratitude to my family for their unwavering support. And lastly, a heartfelt thank you to my incredible friends who bring excitement to my life. I also want to express my gratitude to all my contemporaries whom I haven't directly interacted with, for indirectly influencing building of my character and principles.

1. Introduction

Organic-inorganic metal halide perovskites are excellent optoelectronic materials. Among them, 2D layered perovskites can have limitless combinations of various organic cations and anionic inorganic layers, yielding novel functionalities along with structural diversity.[1] 2D perovskites are lower dimensional (electronic) congeners of 3D perovskites that have general formula of ABX_3, where A and B are two different sized monovalent and divalent cation respectively. Whereas, X is anion coordinated to divalent cation B together forming BX_6 octahedra.[2] Such octahedra connect with each other in the corner sharing fashion and build the 3D framework, hence the name "3D perovskite". The larger cation A occupies the space in between the cavities formed by eight corner sharing octahedra (Figure 1).[2] Substituting A-site cation with large organic cation (with effective size more than 2.6 Å/ more than three C-C bonds) breaks the corner sharing connection in a direction giving rise to organic-inorganic layered 2D perovskite structures with general formula of A_2BX_4 (Figure 1).[3] Hybrid organic-inorganic perovskites serve as platform for integrating the characteristics of both chemical domains into a single entity.[4] Organic compounds have diverse properties like structural flexibility and adaptability, while inorganic materials offer benefits such as good electrical mobility and tuneable bandgaps, and heat resistance.

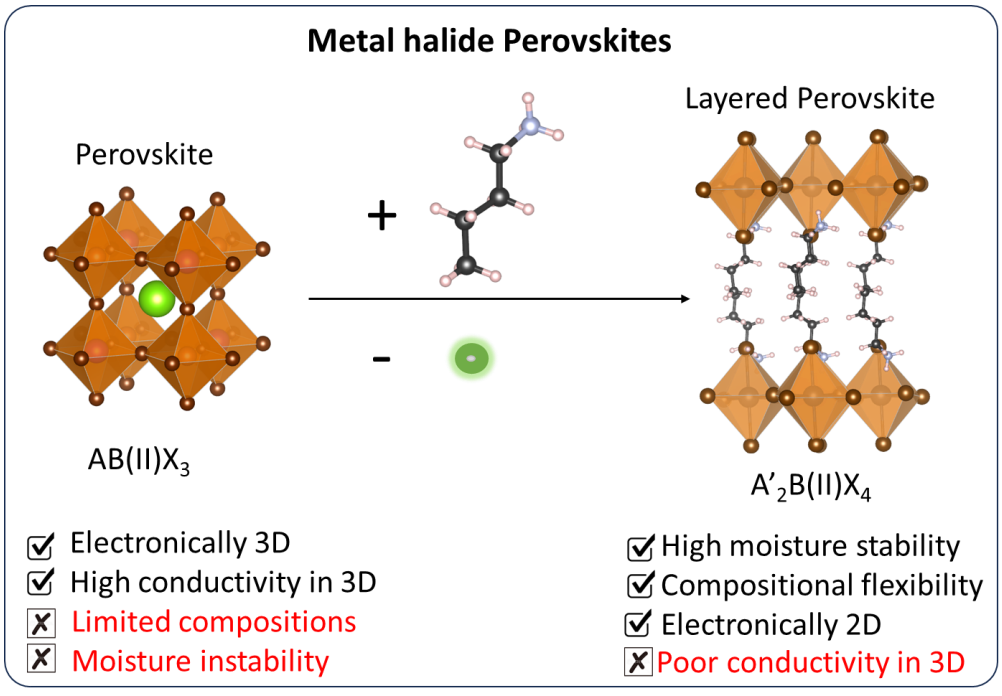

Figure 1: Comparison between 3D perovskite structure 2D perovskite structure. Enlist below are comparative advantage (black) and drawbacks (red) arising from their structure.

The specific arrangement of alternating organic−inorganic layers in 2D perovskites generates a ordered 2D multiple-quantum-well (MQW) electronic structure that forms naturally in a bottom-up fashion through self-assembly.[2] Due to this quantum confinement, it provides opportunity to tune bandgap of material with thickness of inorganic layer which is essential in building functional optoelectronic materials. Apart from quantum confinement layered arrangement of organic-inorganic material provides additional dielectric confinement which increases exciton binding energy and facilitates intense photoluminescence at room temperature.[5] Due to these desirable characteristics, needed in high-performance optoelectronics, 2D perovskite are in spotlight of current research.[6]

Typical A_2PbBr_4 2D perovskites have an A-site as organic ammonium cations like n-butyl ammonium ($C_4H_9NH_3^+$), as shown in Figure 2a. Recently, a new kind of hybrid A-site cation layer $[(4AMTP)PbBr_2]_2^{2+}$ was reported, where the organic 4-aminomethyl tetrahydropyran (4AMTP) ion is covalently bound to an inorganic $PbBr_2$ type lattice (Figure 2b).[7–9] The 2D layered perovskite formed using the hybrid A-site cation is $[(4AMTP)PbBr_2]_2PbBr_4$, as shown in Figure 2c. The hybrid A-site layer $[(4AMTP)PbBr_2]_2^{2+}$ has very different chemical bonding interactions and crystal rigidity compared to the typical organic A-site cation.

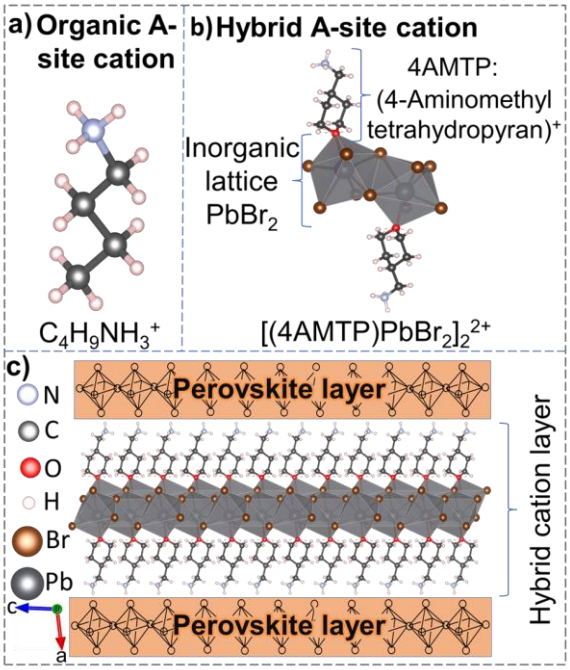

Figure 2: Schematic representation of (a) organic A-site cation butylammonium ($C_4H_9NH_3^+$), and (b) organic-inorganic hybrid A-site cation $[(4AMTP)PbBr_2]_2^{2+}$ where 4AMTP: 4-aminomethyl tetrahydropyran. (c) Schematic representation of $[(4AMTP)PbBr_2]_2PbBr_4$ layered perovskite structure formed by using the hybrid A-site cation.

Karunadasa and coworker reported the hybrid A-site cations for the first time in the year 2021.[9] They viewed the structure as a heterostructure involving the layered perovskite $[PbBr_4]^{2-}$ and layered non-perovskite $PbBr_2O$ lattice (see Figure 2c). If the chemical compositions of both layers can be controlled, then the interactions between such layers have the potential to tailor electronic, optical and magnetic properties. However, till date the chemical compositions remained rather limited,[9] and the full chemical space for this structure-type is not yet revealed.

Inch-sized single crystals and films of $[(4AMTP)PbBr_2]_2PbBr_4$ have been prepared, exploring their luminescence and photodetector properties.[7,8] It has been found that the valence band maximum and the conduction band minimum are constituted by the $[PbBr_4]^{2-}$ perovskite layer. So, the optical properties of $[(4AMTP)PbBr_2]_2PbBr_4$ largely resemble that of typical A_2PbBr_4 with organic A-site cations. However, it has also been suggested that the non-perovskite $PbBr_2O$ layer of the hybrid A-site cation might enhance the photodetector sensitivity for polarized light.[8] It is expected that the hybrid A-site cation layer, either directly, or indirectly through structural modification, would affect the optoelectronic properties of $[(4AMTP)PbBr_2]_2PbBr_4$. So, the exploration of the temperature-dependent structure-property relationship of this newly discovered 2D perovskites is highly desired.

The usual A_2PbX_4 (X = Cl, Br, I) perovskites like $[CH_3(CH_2)_nNH_3]_2PbI_4$ often show phase transition with varying temperatures.[10,11] The $–NH_3$ end of organic A-site cations is anchored to the $[PbX_4]^{2-}$ perovskite layer through hydrogen bonding, but the loose alkyl chains can undergo conformational changes with temperature, driving the structural phase transitions. Interestingly, such phase transitions get suppressed in $(I-(CH_2)_n-NH_3)_2PbI_4$ (n = 2−6) 2D perovskites, where the A-site cation $I–(CH_2)_nNH_3^+$ gets anchored to two adjacent $[PbX_4]^{2-}$ perovskite layers through both $–NH_3$ head and –I tail groups via hydrogen and halogen bonding interactions, respectively.[12] The anchoring of the A-site cation at both end reduces conformational degrees of freedom. In $[(4AMTP)PbBr_2]_2PbBr_4$, the –O end of 4AMTP is covalently bound to a non-perovskite $PbBr_2$ like lattice, and the $–NH_3$ end gets anchored to the $[PbBr_4]^{2-}$ perovskite layer through hydrogen bond (Figure 1c). Apparently, the hybrid A-site cation layer appears to have reduced conformational degree of freedom compared to a typical organic A-site cation, which might lead to suppression of phase transitions in $[(4AMTP)PbBr_2]_2PbBr_4$.

Till date, the possibility of temperature dependent phase transitions in $[(4AMTP)PbBr_2]_2PbBr_4$ and its influence on optical properties have not been explored. Here we employ temperature-dependent single crystal X-ray diffraction (XRD), powder XRD, and photoluminescence (PL) to explore the structure-property correlation. The results show the suppression of phase transition of $[(4AMTP)PbBr_2]_2PbBr_4$ in the entire temperature range of 6 – 300 K. The finding indicates that the new hybrid A-site cation layer provides structural stability (rigidity) to the 2D perovskites.

2. Methodology

2.1 Chemicals

lead bromide (Sigma Aldrich, 98.0%), hydrobromic acid (TCI chemicals, 48% w/w in H_2O, 99.9%), 4-(aminomethyl) tetrahydropyran (4AMTP) (TCI chemicals, ≥98.0%), diethyl ether (TCI chemicals), conducting silver paste (Sigma Aldrich). All chemicals are used without any further purification.

2.2 Synthesis of single crystals of the $[(4AMTP)\ PbBr_2]_2PbBr_4$

The single crystals of the $[(4AMTP)\ PbBr_2]_2PbBr_4$ are synthesized using a method described by Aubrey et al.[3] Briefly, 3 mmol $PbBr_2$ is dissolved in 3 mL 48% (w/w) aqueous HBr in a 10 mL glass vial. 4AMTP (2.03 mmol, 240 µL) is then added dropwise, and the mixture is stirred till dissolution. The open vial is placed inside a 100 mL thick glass graduated reagent bottle filled with 30 mL of diethyl ether as anti-solvent. The glass bottle is tightly capped and placed in a disturbance-free environment for 24 hours to obtain centimeter-sized crystals (shown in the Figure 3). These crystals have flake-shaped morphology and are transparent under visible light. The obtained crystals are then washed with diethyl ether and were kept in vials covered with aluminium foil to avoid photodegradation.

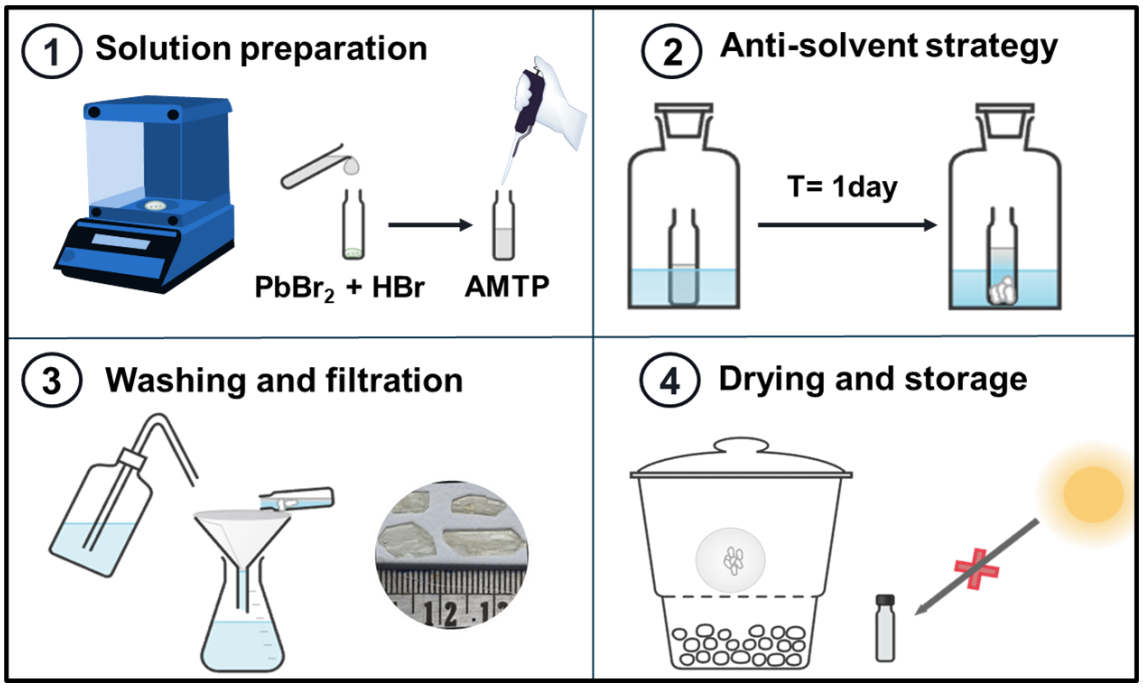

Figure 3: Schematic representation of the synthesis to storage of [(4AMTP) $PbBr_2]_2PbBr_4$ prepared using antisolvent method.

2.3 Instrumental Characterization:

2.3.1 Single Crystal X-ray Diffraction (SCXRD): Single-crystal data were collected using a Bruker Smart Apex Duo diffractometer at 150 K, and 298 K using Mo Kα radiation (λ = 0.71073 Å) as x-ray source. Constant liquid nitrogen flow is maintained towards mounted crystal to collect data at 150 K. The frames at both temperatures were integrated with the Bruker SAINT software package. The well-defined narrow-frame algorithm was employed to integrate the frames. The structures were solved by direct method and refined by full-matrix least-squares on F^2 using the SHELXTL software package. The $PbBr_4$ framework was refined anisotropically without any constraint on Pb and Br atoms. All organic atoms were refined isotropically, and C−C and C−N bond lengths were restrained to ideal values. The obtained structures in form of crystallographic information file (cif) are visualized and analysed in VESTA and Mercury crystal structure viewing softwares.

2.3.2 Powder X-ray diffraction (PXRD): Powder X-ray diffraction (XRD) measurements were carried out on thoroughly ground sample in Bruker D8 Advance X-ray diffractometer employing Cu Kα radiation (1.54 Å) in Bragg-Brentano geometry.

The main principle of XRD pattern formation is based on Bragg's condition,

$$2 \times d \times sin(\theta) = n \times \lambda$$

XRD gives information about the crystal structure, composition of crystals, size of the particles, lattice parameter etc. Temperature dependent PXRD measurements were carried out using Bruker D8 Advance diffractometer equipped with closed cycle helium cryostat to maintain desire temperature and with 1Der strip detector.

Molar volume $V_m(T)$ are calculated as a function of temperature as:

$$V_m(T) = V_T \times N_A/Z,^{13}$$

[where V_T is the volume of the unit cell at temperature T, N_A is Avogadro number and Z is the number of formula unit per unit cell obtained using refined single crystal data.

Coefficient of volume thermal expansion, αv at temperature T is defined as:

$$\alpha v(T) = (1/V_m) \times (dV_m / dT) \text{ (at a constant pressure)}^{13}$$

All diffraction scans are plotted in OriginPro 2023b data analyzing software.

2.3.3 Steady-state photoluminescence (PL) spectroscopy and PL decay dynamics:

Room temperature steady-state photoluminescence (PL) was recorded on FLS980 spectrometer (Edinburgh Instruments). PL decays were collected by time correlated single photon counting (TCSPC) set-up with 375 nm diode LASER (Edinburgh Instruments) as an excitation source. Temperature dependent PL measurements were carried out on FLS980 spectrometer (Edinburgh Instruments). Xe lamp and 375 nm pulsed diode LASER were used as the excitation sources for steady state and time-resolved PL measurements, respectively. Crystal of the sample was attached on sapphire substrate using conducting silver paste was mounted on gold plated sample holder. Required temperature was maintained using closed cycle helium cryostat (Advanced Research Systems) and temperature controller (Lake Shore). The biexponential decay equation has been used to fit PL decay plots is as follow:

$$y = y_0 + A_1 * e^{(-(x-x0)/\tau_1)} + A_2 * e^{(-(x-x0)/\tau_2)} \; ; \; \tau_1 > 0; \tau_2 > 0$$

Where,

y_o = y offset

A_1 = amplitude (contribution) of first exponential part (process) in total fit

A_2 = amplitude (contribution) of second exponential part (process) in total fit

x_o = x offset

τ_1 = time constant of first exponential process

τ_2 = time constant of second exponential process

The Average lifetime (τ_{avg}) for biexponential decay process is calculated from following equation:

$$\tau_{avg} = \left(\frac{A_1 \times \tau_1^2 + A_2 \times \tau_2^2}{A_1 \times \tau_1 + A_2 \times \tau_2}\right)$$

All decay plots are fitted with inbuilt exponential fitting package in OriginPro 2023b data analyzing software. All emission spectra are plotted in OriginPro 2023b data analyzing software.

2.3.5 Thermo-Gravimetric Analysis (TGA):

TGA measurements were carried out using a Perkin Elmer STA 6000. Samples were heated in a temperature range of 30- 600 ºC at a 10 ºC/ min heating rate under inert N_2 flow of 20ml/min. around 3-5 mg of sample is required for TGA measurements.

2.3.6 Differential scanning calorimetry (DSC):

Differential scanning calorimetry (DSC) measurements were carried on Mettler Toledo DSC823 system in the temperature range of -50^{o}C to 235^{o}C in N_2 atmosphere with heating and cooling rates 5^{o}C/min. around 3-5 mg of sample is taken in standard aluminium DSC pan.

3. Results and Discussion:

Following synthesis protocol mentioned in experimental section 2.2 we obtained centimeter sized crystal flakes (see Figure 4). The SCXRD measurement were carried out on these crystals to determine the precise crystal structure for [(4AMTP) $PbBr_2]_2PbBr_4$. Single crystal XRD measurements are carried out at 298 K and 150 K. At 298 K [(4AMTP)$PbBr_2]_2PbBr_4$ crystallizes in $P2_1/c$ space group (monoclinic) with lattice parameter equals to a = 22.26 Å, b = 8.41 Å , c = 7.91 Å and β = 99.04^o. The crystal structure refinement parameters are shown in Table 1. The refinement of crystal data at both temperature is done by Mr. Parikshit Kumar Rajput. The obtained structure agrees with the prior report.[9] The crystal structure shows a layered

arrangement in which an insulating organic layer has been sandwiched between a perovskite layer ($[PbBr_4]^{2-}$; orange color) and a non-perovskite $PbBr_2$ layer (gray color) (see figure 5a). Figure 5b shows a magnified view of the structure. In the hybrid A-site cation $[(4AMTP)PbBr_2]_2^{2+}$, 4AMTP binds to $PbBr_2$ layer by forming a Pb−O covalent bond with bond length 2.7 Å. Thus, Pb in A-site layer has seven coordination (one Pb−O and six Pb−Br bonds) in decahedron geometry, forming $PbBr_2O$. Therefore, the inorganic $PbBr_2O$ lattice in A-site are highly distorted, compared to the regular $PbBr_2$ structure. These decahedra are connected in a layer through edge-sharing. In difference, the anionic $[PbBr_4]^{2-}$ perovskite layer shows the corner-shared octahedra, similar to that of typical 2D layered perovskites with organic A-site cation. The Pb–Br–Pb bond angle in the perovskite layer is found to be 151.7° at 298 K, as shown in Figure 5c. This bond angle is a significant deviation from the ideal 180° Pb–Br–Pb angle. Overall, the structure appears more like a Dion–Jacobson (DJ) phase.[7]

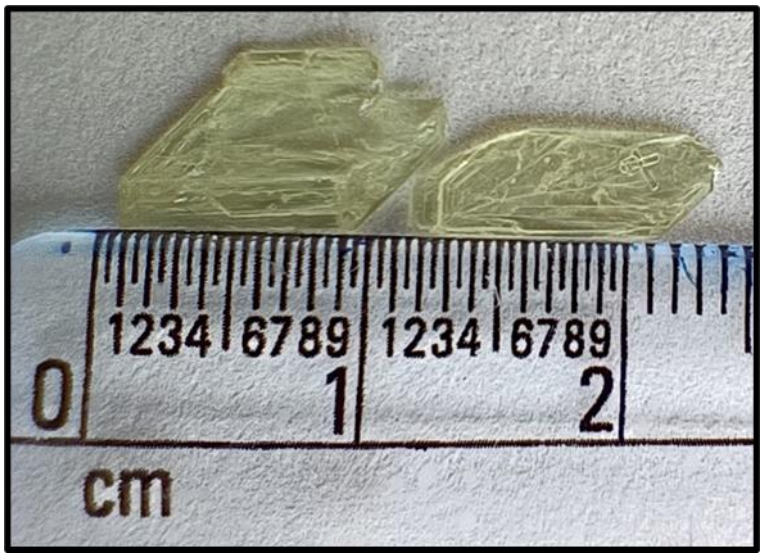

Figure 4: The digital centimetre sized crystal (along with scientific ruler) obtained through antisolvent method.

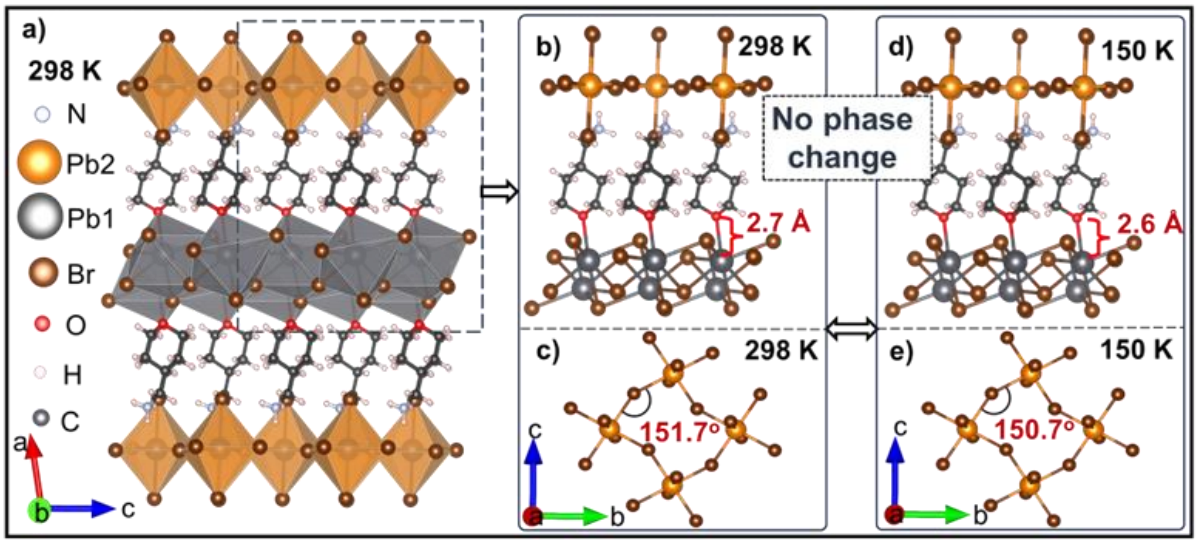

Figure 5: a) The crystal structure of [(4AMTP) $PbBr_2$]$_2$$PbBr_4$ obtained by solving single crystal XRD data at 298 K. Two kinds of Pb atoms are shown: Pb1 (gray spheres) are in hybrid A-site cation, and Pb2 (orange spheres) are in perovskite layer. (b) Magnified view of a part of the structure shown inside the dashed rectangle in (a). (c) Arrangements of Pb and Br in the perovskite layer showing Pb-Br-Pb angle at 298 K. (d) Magnified view of a part of the structure at 150 K, comparing with the data at 298 K shown in (b). (e) Pb and Br arrangement in the perovskite layer at 150 K.

Table 1: Crystallographic data and structural refinement details for [(4AMTP)$PbBr_2$]$_2$$PbBr_4$ at 150 K and 298 K. The refinement of crystal data at both temperature is done by Mr. Parikshit Kumar Rajput.

Sample	[(4AMTP)$PbBr_2$)$_2$$PbBr_4$]	
CCDC Number	2342190	2342189
Temperature	150 K	298 K
Chemical formula	$C_{12}H_{28}N_2O_2Pb_3Br_8$	
Formula weight	1493.16 g/mol	
Wavelength	0.71073 Å	
Crystal system	Monoclinic	
Space group	$P2_1/c$	
Unit cell dimensions	a = 22.1849(12) Å b = 8.3759(5) Å c = 7.8891(5) Å β = 99.119(2)°	a = 22.257(12) Å b = 8.413(5) Å c = 7.911(4) Å β = 99.043(17)°
Volume	1447.41(15) Å^3	1462.8(14) Å^3
Z	2	2
Density(calculated)	3.426 g/cm^3	3.390 g/cm^3
Absorption coefficient	28.459	28.160
F(000)	1312	1312

Theta range for data collection	2.603° to 24.998°	2.592° to 24.995°
Index ranges	-24<=h<=26 -9<=k<=9 -9<=l<=9	-26<=h<=24 -10<=k<=9 -9<=l<=9
Reflections collected	33144	10347
Independent reflections	2545	2563
Coverage of independent reflections	99.9%	99.8%
Absorption correction	Multi-scan	
Structure solution technique	Direct methods	
Structure solution program	SHELXT 2014/5 (Sheldrick, 2014)	
Refinement method	Full-matrix least-squares on F^2	
Refinement program	SHELXL-2018/3 (Sheldrick, 2018)	
Function minimized	Σ w $(F_o^2 - F_c^2)^2$	
Data/restraints/parameters	2545/0/125	2563/0/126
Goodness of fit on F^2	0.864	0.861
Final R indices; I>2σ(I) All data	R1 = 0.0221 wR2 = 0.0507 R1 = 0.0243 wR2 = 0.0518	R1 = 0.0515 wR2 = 0.1302 R1 = 0.0737 wR2 = 0.1521
Weighting scheme	$w = 1/[\sigma^2 (Fo^2) + (0.1000P)^2]$; $P=(Fo^2+2Fc^2)/3$	

In order to check the effect of temperature on crystal structure, we compare the single crystal XRD data measured at both room temperature and 150 K. The refinement parameters at 150 K are shown Table 1. Figure 5d-e shows the magnified view of the $[(4AMTP)PbBr_2]_2PbBr_4$ structure at 150 K. The sample retains the same structure with $P2_1/c$ space group (monoclinic) at 150 K, similar to that in room temperature. The absence structural phase transition in the temperature range of 298 – 150 K is unusual for a typical 2D hybrid perovskite, and we attributed this absence to the rigidity of the hybrid-A site cation of $[(4AMTP)PbBr_2]_2PbBr_4$. Though the crystal phase remains same, the lattice parameters contract at lower temperatures, decreasing the unit cell volume as shown in Table 1. The Pb–O bond length decreases to 2.6 Å, and the Pb–Br–Pb bond angle in the perovskite layer decreases to 150.7º at 150 K, as highlighted in Figure 5d and 5e, respectively. Like-wise, minor changes are there in the penetration depth of $–NH_3$ and N-H···Br hydrogen bonding interactions at 298 K and 150 K, as shown in Figure 6 and table 2.

Table 2: Important structural parameter for $[(4AMTP)PbBr_2)_2PbBr_4]$ at 150 K and 298 K.

Temperature	Penetration Depth	Hydrogen Bonding Interactions	Pb-Br-Pb Bond Angle (°)
(150 K)	0.495 Å	H_c = 2.4483 (7) Å [173.1° (3)]	150.8° (3)
		H_b = 2.5084 (7) Å [168.0° (4)]	
(298 K)	0.484 Å	H_c = 2.512 (3) Å [162.1° (9)]	151.79° (6)
		H_b = 2.552 (3) Å [159.4° (3)]	

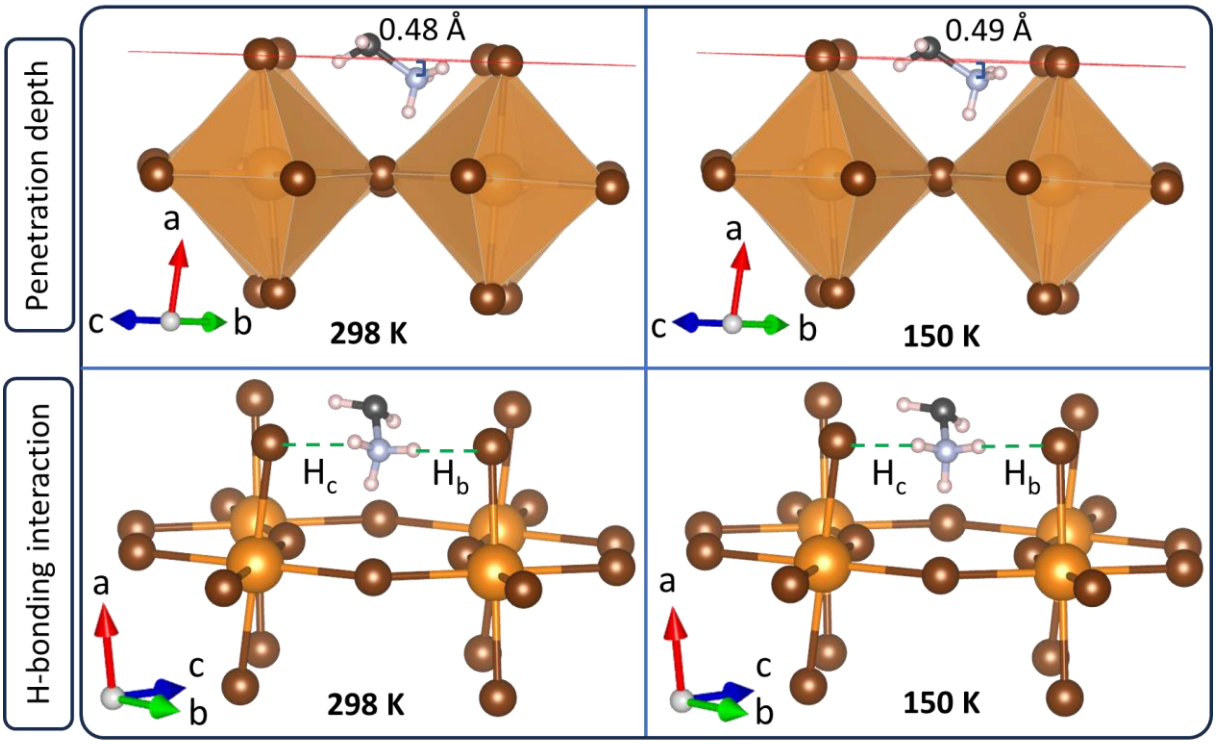

Figure 6: Penetration depth and hydrogen bonding interaction in $[(4AMTP)PbBr_2]_2PbBr_4$ at 298 K and 150 K. H_b and H_c represents H bonding interaction between H and Br atom parallel to b and c axes respectively.

To ensure the results obtained are not due to incomplete thermalization, we carried out low temperature powder x-ray diffraction measurements. Figure 7a shows that the powder XRD pattern of $[(4AMTP)PbBr_2]_2PbBr_4$ matches well with the simulated pattern obtained from its single crystal XRD data. No impurity phase is observed in the powder XRD pattern, confirming the phase-purity of the entire sample. Then we measured the powder XRD data in the temperature range of 298 – 20 K. Pseudo color maps in Figure 7b shows that the powder XRD patterns remains largely unchanged throughout the entire temperature range. The absence of any temperature-dependent phase transition is attributed to the rigid hybrid cation $[(4AMTP)PbBr_2]_2^{2+}$. Both ends of the

organic 4AMTP is bound to inorganic lattices, as shown in Figure 5b. One end to $PbBr_2$ lattice via a Pb-O covalent bond, and the other end to the $[PbBr_4]^{2-}$ perovskite layer through hydrogen bonding. This binding of 4AMTP at both ends provide structural rigidity suppressing the temperature-induced phase transition, similar to previously reported $I\text{-}(CH_2)_n\text{-}NH_3^+$ (n = 2-6) A-site cations that bind through both –I and $–NH_3$ ends.[12] In the absence of phase transition. the only temperature-dependent changes observed is the lattice contraction at lower temperatures. Figures 7c shows that the diffraction peaks systematically shift to higher 2θ values with decreasing temperature, indicating lattice contraction.

To estimate change in volume accompanied by change in temperature quantitively, we calculated volume expansion coefficient. The molar volume of the compound increases linearly with temperature and linear fit for the data has slope of 0.0203×10^{-4} (See Figure 8). Volume expansion coefficient at room temperature is 1.3908×10^{-4} K^{-1}.

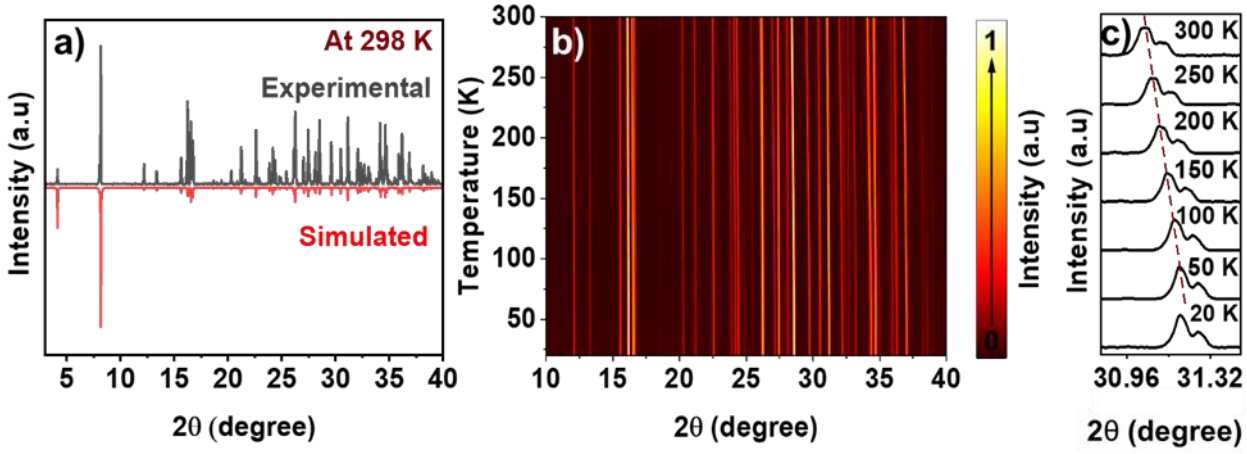

Figure 7: a) PXRD pattern of $[(4AMTP)\ PbBr_2]_2PbBr_4$ experimental and simulated shows phase purity of obtained sample. b) Pseudo color map showing temperature-dependent (300 –20 K) experimental powder XRD patterns of $[(4AMTP)PbBr_2]_2PbBr_4$ in the 2θ range of 10^o to 40^o. c) A magnified view of temperature-dependent powder XRD patterns showing systematic contraction of the lattice at lower temperatures.

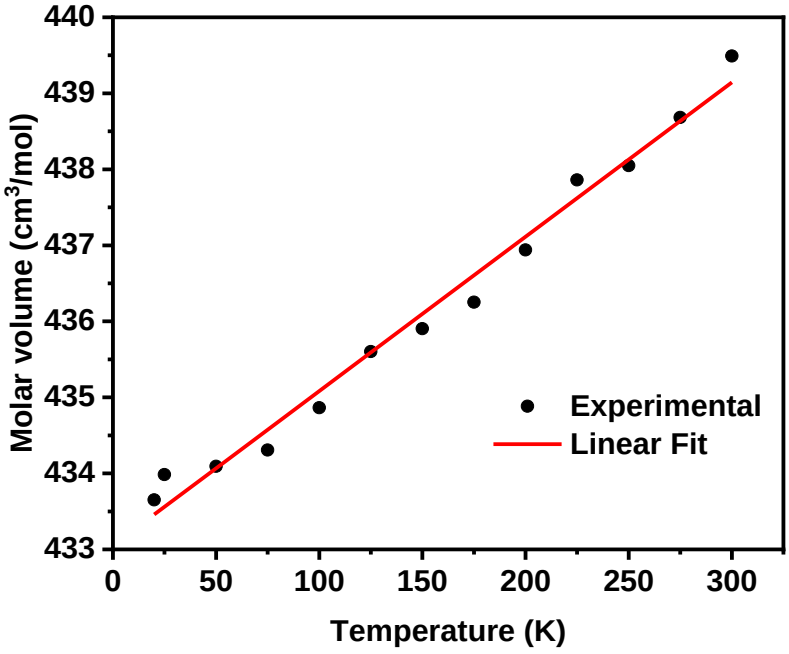

Figure 8: Change in molar volume of crystal with temperature. The molar volume of the compound increases linearly with temperature and linear fit for the data has slope of 0.0203X 10-4.

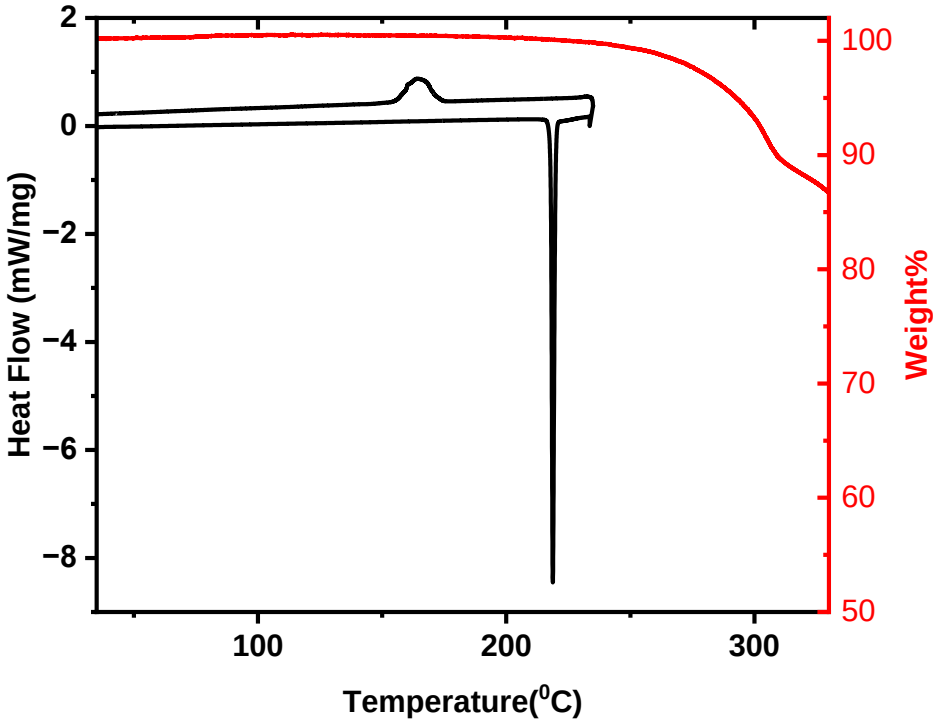

Figure 9: TGA and DSC plots of [(4AMTP) $PbBr_2]_2PbBr_4$ from room temperature to 330°C. the TGA plots suggest that sample experience 0.1% weight loss at 226°C. the sharp peak in heating curve of DSC measurement corresponds to melting of the sample.

These studies indicates that the hybrid cation provides structural rigidity to overall structure and thus suppressing solid-solid phase transition. To get know whether the hybrid cation can provide structural stability over thermal decomposition, we performed thermal gravimetric analysis and differential scanning calorimetry measurements (Figure 9). The results show that hybrid cation provides structural stability to the compound till 240^{o}C (0.3% weight loss). it is found that the compound shows solid-liquid transition (melting) around 218^{o}C. so, till 218^{o}C there is no solid-solid phase transition supporting our argument on role of hybrid cation in suppressing phase transition.

A prior report suggested that a monoclinic-phase 2D perovskites might lead to the observation of a spin-forbidden “dark exciton” emission with a long PL emission lifetime.[14] Furthermore, at the lower temperatures, the nature of PL of 2D hybrid perovskites often changes, even with appearance of a new lower energy peak attributed to self-trapped exciton emission.[14] Also, any possible temperature-dependent phase transition might get reflected in the PL. But such PL measurements of [(4AMTP)$PbBr_2$]$_2$$PbBr_4$ at cryogenic temperature have not been reported so far. In order to get those insights, we carried PL measurements in the temperature range of 300 – 7 K.

The temperature-dependent structural phase transition typically changes the band gap of the materials and, thereby, the optical properties of it.[11] In case of 2D perovskite structural transition brings drastic change in position of excitonic peak.

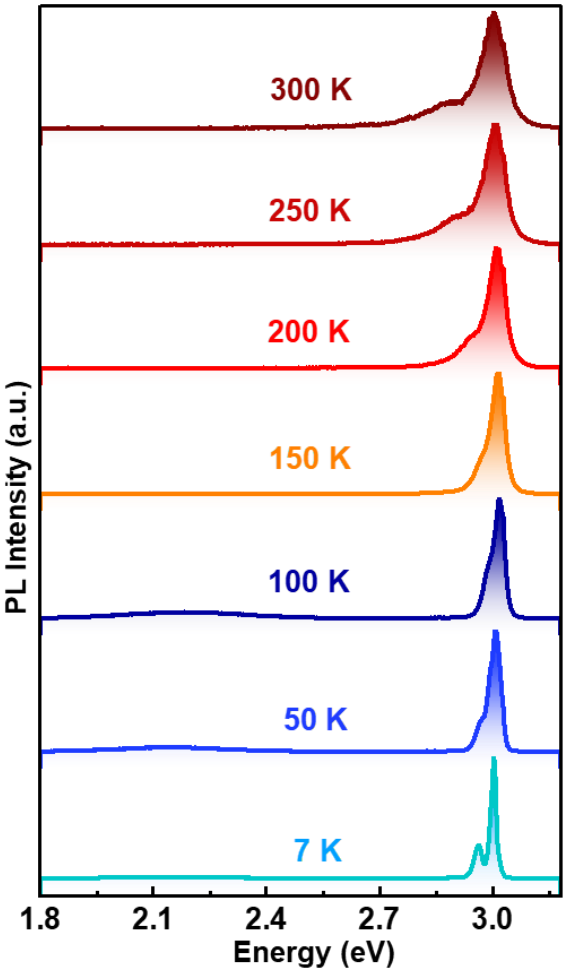

Figure 10: Normalized photoluminescence spectra of of [(4AMTP) $PbBr_2$]$_2$$PbBr_4$ in 7-300 K temperature range.

Despite the different chemical architecture, [(4AMTP) $PbBr_2$]$_2$$PbBr_4$ single crystal shows dual emission peaks similar to 2D perovskites at room temperature (300 K) (Figure 10). This is mainly because the incorporated $PbBr_2$ layer does not contribute to CBM and VBM in the electronic band structure. Following the dual exciton model, the sharp, narrow, higher energy peak at 3.002 eV and a lower energy peak at 2.883 eV are assigned to the edge and interior exciton respectively. PL decay curves measured at respective energy of emission shows that both of emission have similar lifetimes at 275 K (at 300 K PL decay curves lie closer to IRF, so decay curves at this temperature are less reliable in interpreting lifetime values) (Figure 11). The spectrum at 300 K (Figure 10a) also shows the tailing of low energy excitonic peak, mainly described in literature due to exciton-phonon coupling.[15]

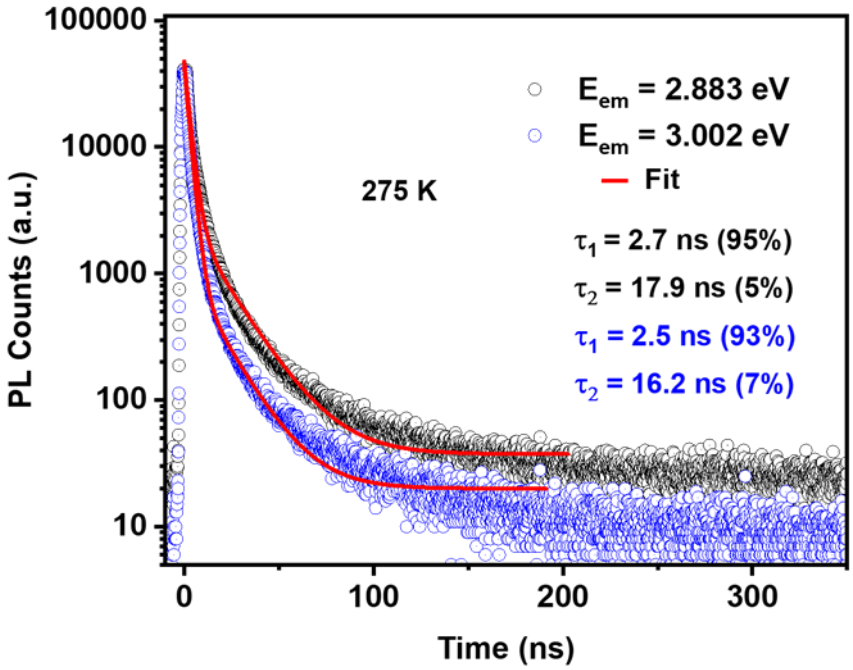

Figure 11: PL decay for two of the excitonic features along with their fitting parameters at 275 K.

On lowering the temperature, the higher energy excitonic peak 3.002 eV does not show any abrupt shift with temperature (see Figure 10), indicating that the sample does not show any phase change through the structure-property relationship. However, the lower energy excitonic peak shows a blue shift with a lowering temperature until it merges partially with a higher energy peak at 100 K (See Figure 10). Such blue shift of emission peak has been reported earlier in the case of $(BA)_2PbBr_4$, $(MHZ)_2PbBr_4$ but the explanation of such behavior is still unclear in literature.[16,17]

Such type of 2D perovskite that crystallizes in monoclinic space group and that does not show phase transition often shows unusually high lifetimes for excitonic emission at cryogenic temperatures (below 100 K), attributed to contribution from dark excitonic states.[14] The dark excitonic state has high lifetime (from 200ns to as high as few µs) due to spin forbidden transition. Contribution is significant as this state lie very close to usual bright excitonic states (corresponding to spin allowed transition) (16 to 23 meV below the bright state)[14]. For $[(4AMTP)\ PbBr_2]_2PbBr_4$, we observed red shift of ≈ 15 meV (Figure 12 a,b) below 50 K . PL decay curves measured at these peak positions shows the comparatively longer decay dynamics at 7 K than 100 K (Figure 4c,d).

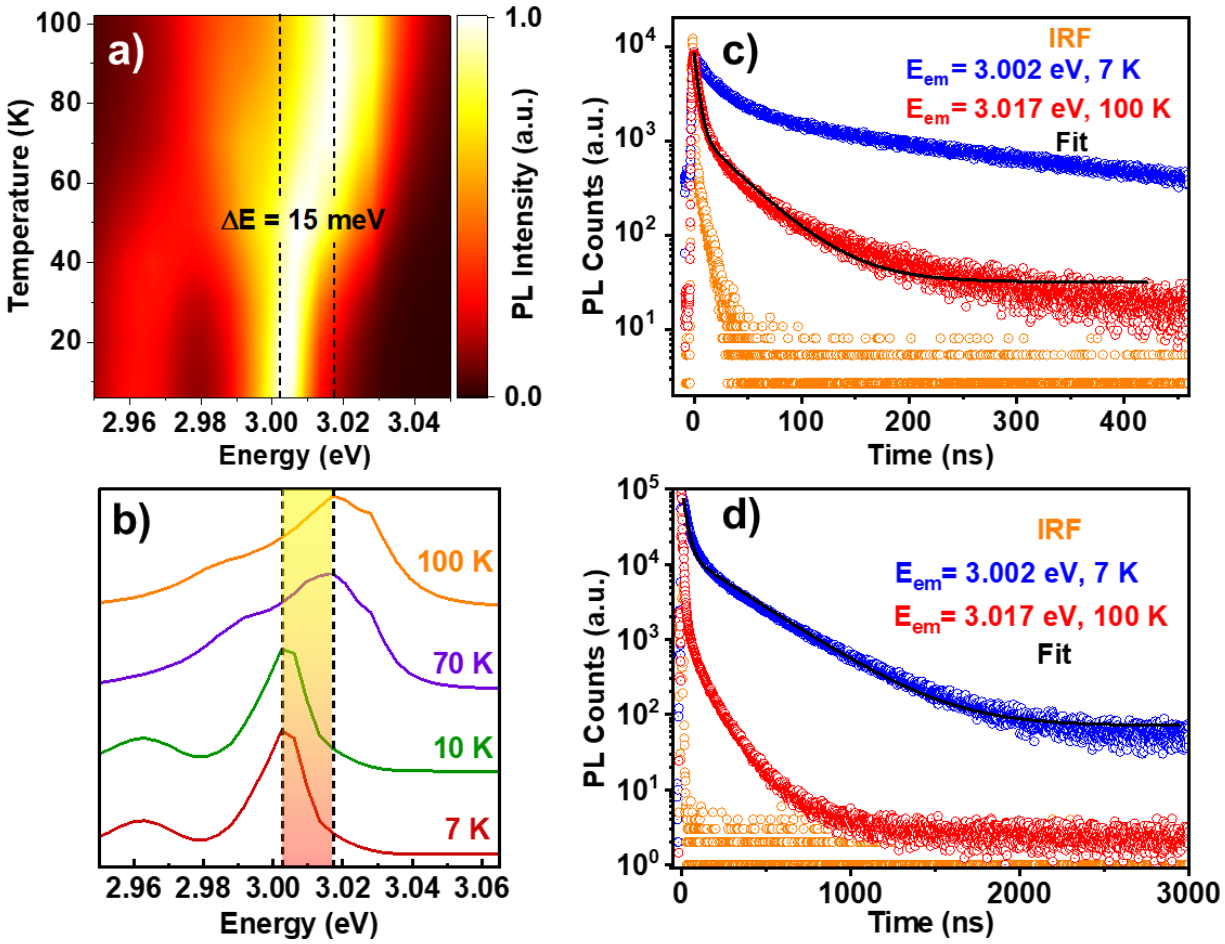

Figure 12: a) Colormap of temperature-dependent PL spectra of [(4AMTP) $PbBr_2]_2PbBr_4$ featuring different optical features in 7 to 100 K. ΔE represents energy difference between two excitonic states. b) Photoluminescence spectra at four different cryogenic temperature. c,d) PL decay plots measured at 3.002 eV and 3.017 eV for 100 K and 7 K in pulse period of 500 ns and 3000ns.

These observations can be best described through three state model schematics shown in figure 13. If the thermal energy (k_BT) is insufficient in back transfer of population to higher energy state then contribution from low energy state having high lifetime increases and vice versa. Situationally, we observed biexponential decay profiles in those temperatures at respective peak positions (Figure 14) and corresponding fitting parameters are shown in table 3 respectively.

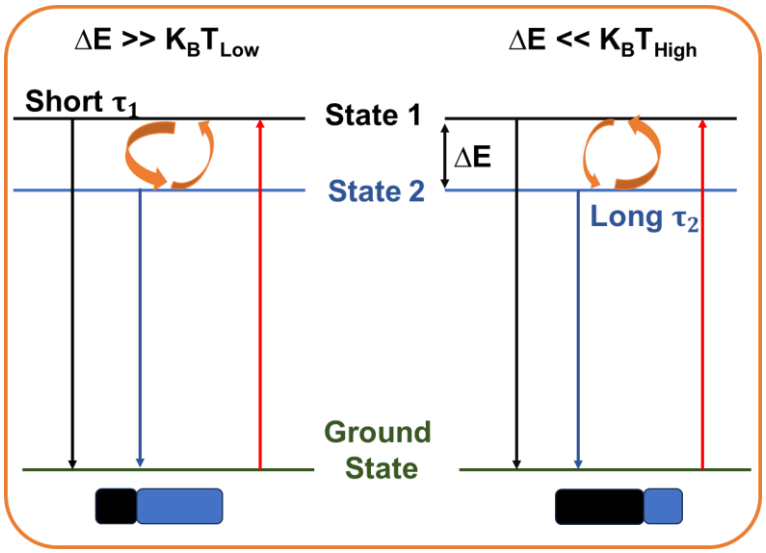

Figure 13: Three state model schematics. The state 2 (blue) corresponds to long lived excitonic state where as state 1 (black) corresponds to comparatively short lived excitonic state. The amount of excited state molecules that will reside in two of this state depends on temperature and fixed ΔE value between two states. At high temperature emission obtained will have more contribution from state 1 and vice versa. The size of black and blue rectangles at bottom of figure show estimation of contribution during deexcitation.

.

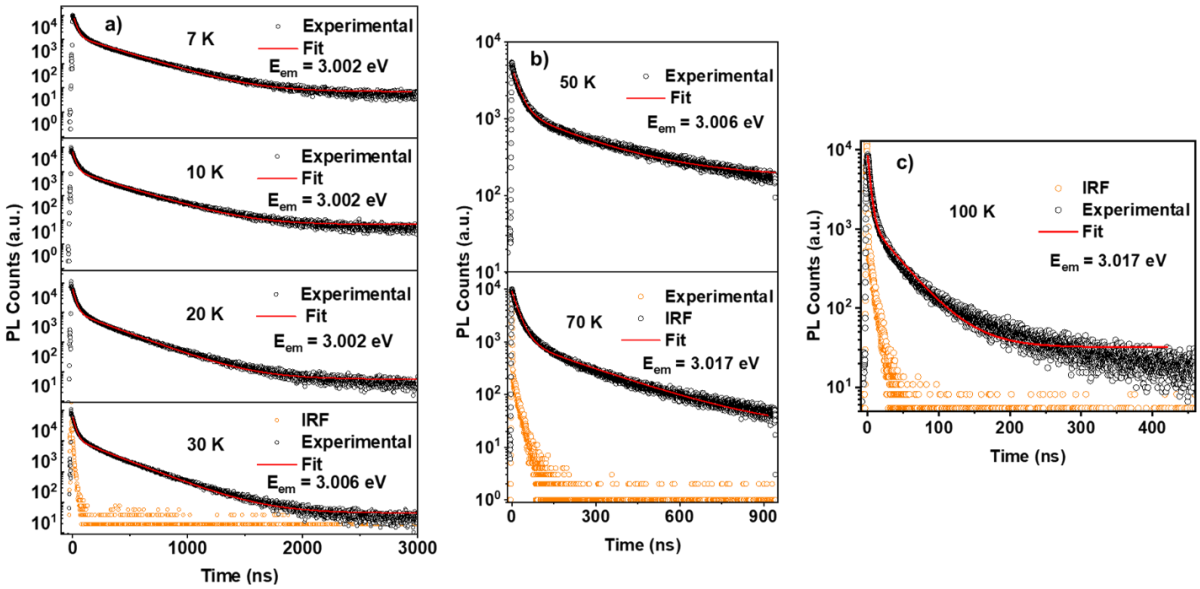

Figure 14: PL decay plots along with fitting measured at peak position in 7- 100 K temperature range. In temperature range of 7- 30 K decay curves are measured in 5us pulse period. At 50K and 70 K decay curves are measured in 1us pulse period and at 100 K PL decay curve is measured in 500 ns pulse period.

Table 3: The biexponential fitting parameters obtained for PL decay curves in Figure 14.

Temperature (K)	A_1%	τ_1 (ns)	A_2%	τ_2 (ns)	τ_{avg} (ns)	R-Squared (COD)
6 K	7	24.3	93	298.0	296.4	0.993
10 K	17	24.3	83	298.7	294.1	0.991
20 K	24	24.3	76	298.0	291.2	0.994
30 K	31	24.5	69	298.0	288.4	0.996
50 K	77	26.9	23	250	190.8	0.997
70 K	95	24.3	5	230.8	90.8	0.993

At high cryogenic temperatures (70 K and 100 K) after excitation, excited molecules get relaxed to lower energy. Since this state has high lifetime (around 250- 300 ns), molecules residing in this state get sufficiently more duration to get thermal excited to high energy state than to depopulate from long lived state. These get reflected in PL decay curves measured at peak emission position in terms of increment in amplitude or contribution of state 1 (A_1%) and decrease in amplitude or contribution of state 2 (A_2%). The quantitative increase in average lifetime and contribution with lowering temperature has been summaries in figure 13a and 13b respectively. nearly 3-fold increase in average lifetime has been observed.

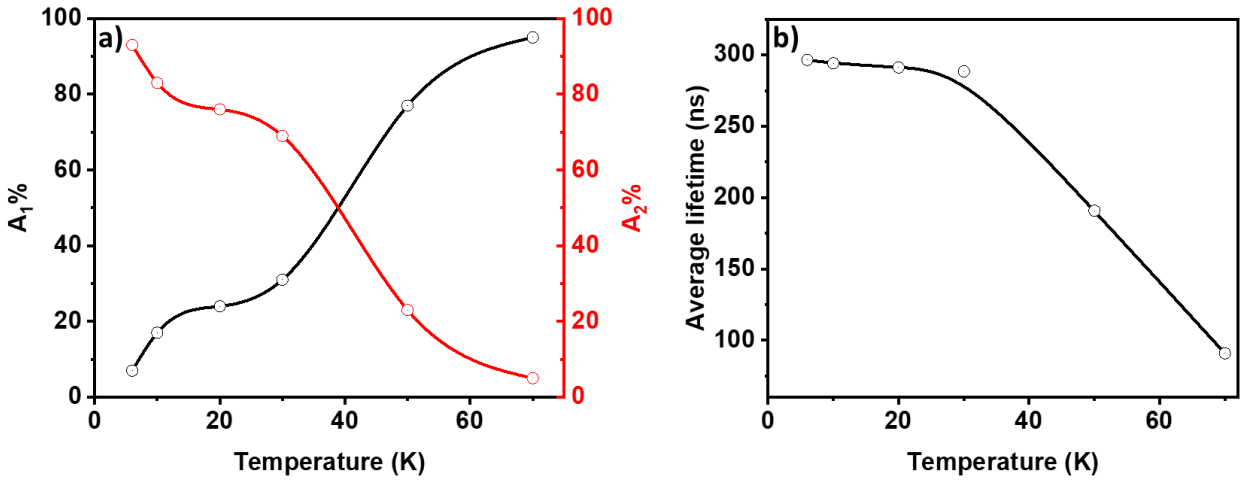

Figure 15: a) Variation of percentage contribution from state 1 (red) and state 2 (black) with temperature. b) Variation in calculated average lifetime with temperature. the average lifetime increases with increase in contribution from state 2.

Above 100 K, there is no significant contribution from state 2. This is also evident from PL decay curves measured above 100 K at peak positions (Figure 14). fitting of these PL decay curves indicates presence of small lifetime component (Similar to state 1) whose value varies from 30 ns to 14 ns (Table 4).

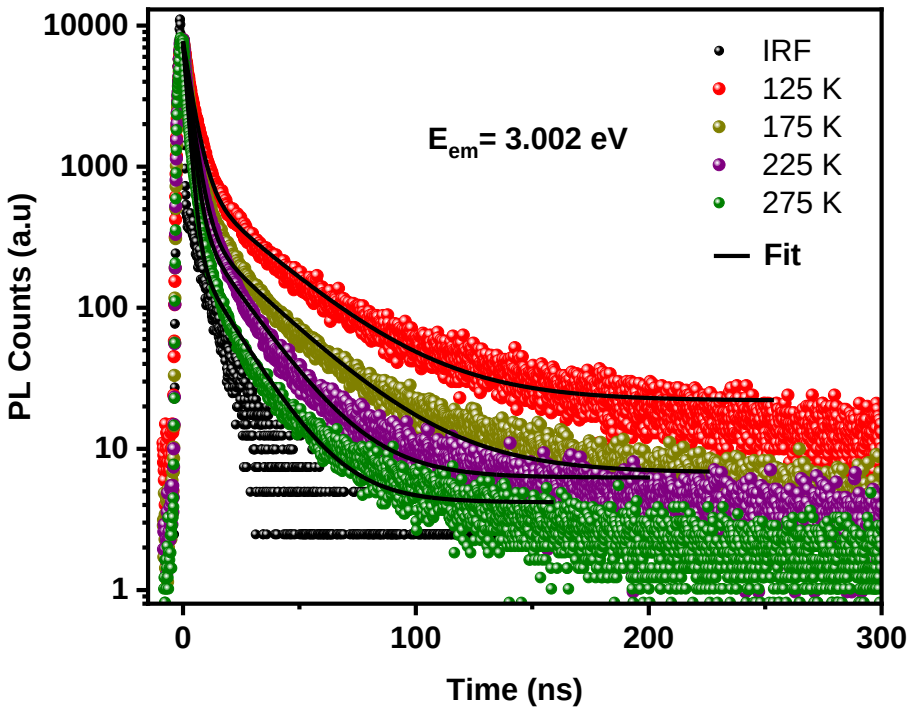

Figure 16: PL decay curves measured at high energy excitonic peak position for temperature range of 125- 300K.

Table 4 : PL decay fitting parameter for excitonic emission in 125-300 K.

Temperature (K)	A_1%	τ_1 (ns)	A_2%	τ_2 (ns)	τ_{avg} (ns)	R-Squared (COD)
125 K	90	10	3.8	30	15.8	0.998
150 K	94	6	3.8	30	12.5	0.992
175 K	94	6	3.2	27.5	11.3	0.990
200 K	93	7	2.9	20.0	8.5	0.992
225 K	94	6	2.5	18.4	7.6	0.990
250 K	96	4	2.1	16.1	5.8	0.990
275 K	96	4	1.9	15.9	5.2	0.990
300 K	97	3	1.3	14.1	4.4	0.990

In temperature range 50 K to 125 K, we observed a weak broad emission centered at 2.126 eV (see Figure 10: 50 K, 100 K). Such broad, low energy emission than excitonic

emission has been observed for all other hybrid perovskite lead based system and has been previously described as self-trapped exciton (STE) emission.[14] The intensity of this emission is maximized at 70 K and decrease subsequently (Figure 15; red curve). We have record PL lifetime for this emission to confirm its STE nature (Figure 16). The fitting parameters with respect to fitting is mentioned in table 5. The time constants obtain after biexponential fitting lies in µs. this further confirms STE nature.

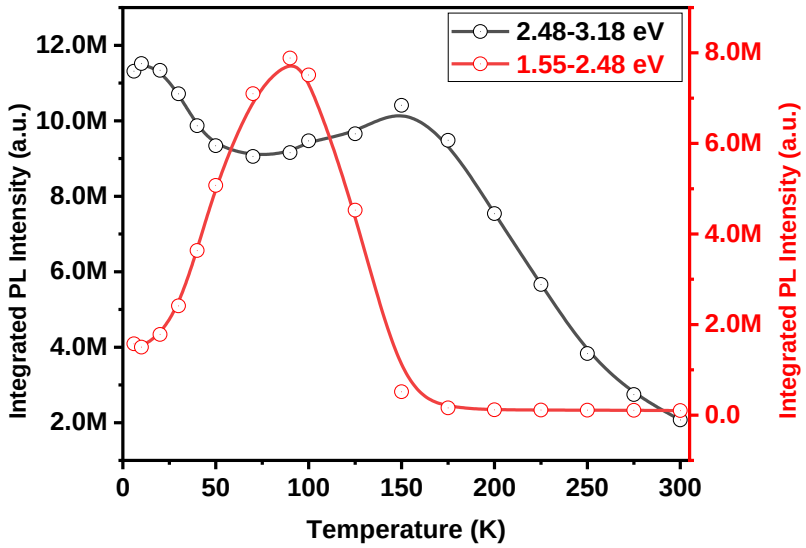

Figure 17: Integrated PL Internsity for broad STE emission (1.55-2.48 eV) shown by red curve. The intensity is maximum at 70K. Black curve show variation of integrated PL of excitonic peaks with temperature.

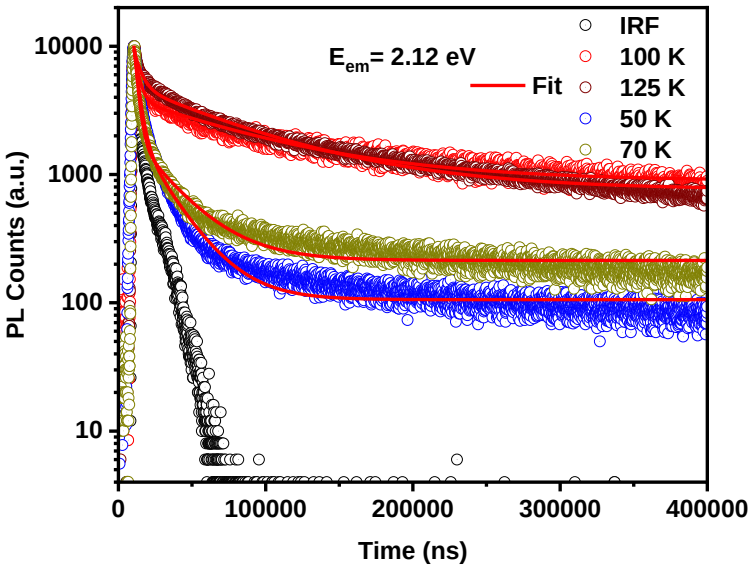

Figure 18: PL decay curves measured at STE peak position for temperature range of 50-125 K.

Table 5: PL decay fitting parameters for STE emission.

Temperature (K)	A_1%	τ_1 (ns)	A_2%	τ_2 (ns)	τ_{avg} (ns)	R-Squared (COD
50 K	82	7080	17	84572.788	62733.58	0.997
70 K	76	5099.3079	23	82118.666	69304.31	0.992
100 K	85	3392.0113	14	84280.237	68964.73	0.976
125 K	88	4962.0689	11	84114.28	59976.47	0.991

4. Conclusion:

We were successful in synthesizing phase pure [(4AMTP) $PbBr_2]_2PbBr_4$ through antisolvent method. The crystal structure obtained through refinement of single crystal x-ray diffraction data at 300 K suggest layered arrangement in which hybrid cation [(4AMTP) $PbBr_2]_2^{2+}$ and anionic inorganic $[PbBr_4]^{2-}$ are stacked on one another similar to usual 2D layered perovskites, where instead of hybrid cation it has pure organic cation. The comparison of crystal structure at 150 K and 300 K suggest the sample retains the same structure with P_{21}/c space group (monoclinic) at 150 K, and there is no phase transition observed. The penetration depth, hydrogen bond interactions, and other important crystallographic parameters show negligible change in their value with change in temperature. Suppression in phase transition and negligible change in crystallographic parameters directly points to high rigidity provided to structure by hybrid cation.

This suppression of phase transition due to incorporation of hybrid cation has been further verified till cryogenic temperatures through LTPXRD measurements. The volume expansion coefficient calculated from LTPXRD measurement is 1.3908 X 10^{-4} K^{-1} at room temperature.

The absence of any abrupt change in high energy excitonic peak position in low temperature photoluminescence measurement further supports observed suppression in phase transition. The [(4AMTP) $PbBr_2]_2PbBr_4$ 2D perovskite crystallizing in monoclinic space group is found have unusually high excitonic lifetime at cryogenic temperature (below 30 K) attributed to long lived excitonic state (often described as dark exciton). The three states model described for such observation shows increment

in contribution of long lived excitonic state in deexcitation process with lowering temperature. such observation has been previously made for nanocrystals and thin films of 2D perovskites having monoclinic crystal structure. Though very few reports have claimed such observation on single crystal of 2D perovskites. Our study could potentially advance the understanding of photophysical processes observed at cryogenic temperatures in the monoclinic crystal structure of 2D perovskite, that does not show phase transition.

5. References:

1. Nag, A. “Plenty of Room” at the Interface of Hybrid Metal Halide Perovskite Single Crystals. *Nano Lett* **21**, 8529–8531 (2021).
2. Mao, L., Stoumpos, C. C. & Kanatzidis, M. G. Two-Dimensional Hybrid Halide Perovskites: Principles and Promises. *J Am Chem Soc* **141**, 1171–1190 (2019).
3. Shannon, R. D. Revised effective ionic radii and systematic studies of interatomic distances in halides and chalcogenides. *Acta Crystallographica Section A* **32**, 751–767 (1976).
4. Mitzi, D. B. Templating and structural engineering in organic–inorganic perovskites. *Journal of the Chemical Society, Dalton Transactions* 1–12 (2001) doi:10.1039/b007070j.
5. Hattori, T., Taira, T., Era, M., Tsutsui, T. & Saito, S. Highly efficient electroluminescence from a heterostructure device combined with emissive layered-perovskite and an electron-transporting organic compound. *Chem Phys Lett* **254**, 103–108 (1996).
6. Li, X., Hoffman, J. M. & Kanatzidis, M. G. The 2D Halide Perovskite Rulebook: How the Spacer Influences Everything from the Structure to Optoelectronic Device Efficiency. *Chem Rev* **121**, 2230–2291 (2021).
7. Zu, H.-Y., Han, X.-B., Fan, C.-C., Liang, B.-D. & Zhang, W. [(4AMTP)$PbBr_2$]$_2$$PbBr_4$: a Nontypical Cation-Coordinated Perovskite Showing Deep-Blue Emissions and Blue-Light Photoelectric Response. *Inorg Chem* **61**, 17738–17745 (2022).
8. Ma, Y. *et al.* Non-artificial Layered Heterostructure as Inch-size Single Crystal for Shortwave Polarized-Light Array Detector. *Adv Funct Mater* **33**, (2023).
9. Aubrey, M. L. *et al.* Directed assembly of layered perovskite heterostructures as single crystals. *Nature* **597**, 355–359 (2021).
10. Barman, S. & Vasudevan, S. Melting of an Anchored Bilayer: Phase Transitions in the Organic−Inorganic Hybrid Pervoskite (CH_3NH_3)($CH_3(CH_2)_nNH_3)_2Pb_2I_7$ (n = 11, 13, 15, 17). *The Journal of Physical Chemistry C* **113**, 15698–15706 (2009).

11. Sheikh, T., Shinde, A., Mahamuni, S. & Nag, A. Possible Dual Bandgap in ($C_4H_9NH_3)_2PbI_4$ 2D Layered Perovskite: Single-Crystal and Exfoliated Few-Layer. *ACS Energy Lett* **3**, 2940–2946 (2018).

12. Chakraborty, R., Sheikh, T. & Nag, A. Iodine–Iodine Interactions Suppressing Phase Transitions of 2D Layered Hybrid ($I\text{-}(CH_2)_n\text{-}NH_3)_2PbI_4$ (n = 2–6) Perovskites. *Chemistry of Materials* **34**, 288–296 (2022).

13. Ravi, V. K. *et al.* Colloidal $BaZrS_3$ chalcogenide perovskite nanocrystals for thin film device fabrication. *Nanoscale* **13**, 1616–1623 (2021).

14. Shinde, A. *et al.* Emissive Dark Excitons in Monoclinic Two-Dimensional Hybrid Lead Iodide Perovskites. *Nano Lett* **23**, 6985–6993 (2023).

15. Ni, L. *et al.* Real-Time Observation of Exciton–Phonon Coupling Dynamics in Self-Assembled Hybrid Perovskite Quantum Wells. *ACS Nano* **11**, 10834–10843 (2017).

16. Mączka, M. *et al.* $[Methylhydrazinium]_2PbBr_4$, a Ferroelectric Hybrid Organic–Inorganic Perovskite with Multiple Nonlinear Optical Outputs. *Chemistry of Materials* **33**, 2331–2342 (2021).

17. Dutta, T. *et al.* Edge versus Interior Mn^{2+} Doping in 2D Layered Butylammonium Lead Bromide Perovskite Single Crystals. *The Journal of Physical Chemistry C* **126**, 21109–21116 (2022).